Heliyon 10 (2024) e39628

Contents lists available at ScienceDirect

Heliyon

journal homepage: www.cell.com/heliyon

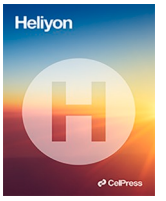

Research article

Application of cloud point extraction coupled with derivative spectrophotometry to remove binary mixture of Cresol Red and Methyl Orange dyes from aqueous solutions: Box–behnken design optimization

Shahnaz Sargazi [a,b], Mohammad Taghi Ghaneian [a], Mashaallah Rahmani [c], Ali Asghar Ebrahimi [a,*]

[a] Environmental Sciences and Technology Research Center, Department of Environmental Health Engineering, School of Public Health, Shahid Sadoughi University of Medical Sciences, Yazd, Iran
[b] Health Promotion Research Center, Department of Environmental Health Engineering, School of Public Health, Zahedan University of Medical Sciences, Zahedan, Iran
[c] Department of Chemistry, Faculty of Sciences, University of Sistan and Baluchestan, Zahedan, 98135-674, Iran

ARTICLE INFO

Keywords:
Anionic dyes
Binary mixture
Box-behnken
Cloud point extraction
Derivative spectrophotometry

ABSTRACT

Cloud point extraction (CPE) was employed to eliminate Cresol Red (CR) and Methyl Orange (MO), as anionic dyes in a binary mixture from aqueous solutions. To remove these dyes Triton X-100 and NaCl at pH 5.7 were utilized. In this vein, wavelengths of 365 nm and 520 nm were respectively selected for CR and MO using the derivative spectrophotometer and first-order derivatives. According to based on the first-order derivative spectrophotometry, the recoveries rised from 94.3 to 99.5 % for CR and from 94.6 to 99.1 % for MO. In the following, the response surface methodology was administered to investigate the effect of surfactant concentration, temperature, and time on the dyes' elimination process. The quadratic mathematical model was obtained from the Box-Behnken design (BBD) matrix and developed to estimate the impact of each variable and its relationship with the elimination parameters. Later, coefficients of determination (R^2) $\geq$0.97 were obtained using model equations and comparison between predicted and empirical values. Analysis of variance estimated the models' significance and anticipation while processing the study variables. Based on the results, the model of pseudo-first-order in kinetic modelling can best describe dyes adsorption among the studied models. The analyzed dyes adhere to the Langmuir model with correlation values of 0.86 for CR and 0.87 for MO. The monolayer capacity (Q_{max}) was determined as 0.77 mol/mol for CR and 26.41 mol/mol for MO.

1. Introduction

Water pollution, caused by improper municipal and industrial wastewater disposal, harmful contaminants, and poor solid waste management, has a detrimental effect on the health of all living beings. Due to the large volume of wastewater entering the water, uninterrupted effort is required to ensure proper wastewater disposal in the ecosystem [1,2]. Colored wastewater discharges from

* Corresponding author.
E-mail address: ebrahimi20007@gmail.com (A.A. Ebrahimi).

https://doi.org/10.1016/j.heliyon.2024.e39628
Received 4 June 2024; Received in revised form 14 October 2024; Accepted 18 October 2024
Available online 28 October 2024

various industries, including textiles, paper, wood, cosmetics, agriculture, plastics, and leather, can lead to serious environmental problems. Due to their exceptional resistance to extreme climatic conditions as a result of their chemical and photocatalytic stability, most dyes pose a significant health risk to all living organisms [3], causing damage to human organs and body systems, including the lungs, liver, Vasco-circulatory system, reproductive system, and immune system. Additionally, they may trigger allergic responses, eczema, and skin dermatosis [4–6].

CR along with MO are negatively charged dyes used as indicators in laboratories. CR, classified as a dangerous substance by Occupational Safety and Health Administration (OSHA) [7], causes irritation to the eyes, respiratory system, and skin. MO as an azo dye, has mutagenic and carcinogenic characteristics [8].

CR and MO dyes similar most commercial anionic dyes have a high solubility and chemical stability in water, allowing them to persist for long periods even when subjected to heat, chemicals, and light [9]. Previous research has described standard methods for separating and removing dyes, such as adsorption [10–20], extraction [21–23], coagulation [24–26], and degradation [27–34]; however, all these methods are faced with limitations, such as 1) the usage of rather costly sorbents, resulting in high preparation expenses and restricted reusability [35]. 2) Non-accessibility of ozone used in the process of ozonolysis. 3) The toxicant impacts of chemical substances necessary for the process of coagulation [14]. To face these challenges researchers have recently developed more effective methods to remove dyes, including anionic dyes.

CPE, as a contemporary and highly effective technique for extracting fluids, involves using surfactants to separate organic and inorganic components in the field of separation science [36]. This approach facilitates separating the hydrophobic and hydrophilic components [37] relying on the clouding phenomenon demonstrated by surfactants [38]. In this regard, the examined solution is divided into two separate phases by heating up to a certain temperature, known as the cloud point temperature (CPT), at which the solution transforms into a surfactant exceeding the critical micellar concentration [39]. When the temperature exceeds the critical micelle temperature (CPT), surfactant molecules form micelles and arrange their hydrocarbon tails inward, creating a nonpolar hydrophobic core. The technique has been employed for removing and measuring metallic elements and dyes [40–49], predicting pharmaceutical drugs [50,51] in food, and analyzing organic chemicals [52].

Furthermore, CPE not only offers reducing solvent exposure but also is highly cost-effective and time-efficient. This method also enjoys an intrinsically safe design with low possibility of risks and accidents, like fires, choking, or explosions, since it does not require using harmful detectors or organic solvents. In other words, CPE is categorized as a green analytical technique because it uses a small amount of nontoxic surfactant (rather than a hazardous organic solvent) [53–57].

There is significant apprehension in analytical chemistry about simultaneous tracing of several dyes in a specimen without separating individual ingredients. To perform simultaneous analysis of dye systems containing many components, spectrophotometry of Ultraviolet–visible (UV–Vis) absorption is a more cost-effective and less complicated method than electrophoresis and chromatography. However, UV–Vis frequently encounters problems because its zero-order absorption spectra overlap. The spectrophotometry with a conventional first-order derivative was utilized to resolve spectral overlaps and remove the signals in the background emanating from the presence of additional elements in the samples [58]. Derivative spectrophotometry offers a wide range of applications in biochemical, clinical, and pharmacological research as well as inorganic and organic analysis [58,59]. The “zero-crossing technique”, as a precise method of data analysis, enables quantitative measurement of an analyte in the sample of a matrix and permits simultaneous detection of two analytes in binary mixtures. Given that derivatization results are influenced by the shape of absorption spectra with zero order, signals are wide, flattened, and then zeroed, amplifying analyte signals. So, the zero-crossing technique provides a proportional amplitude for the derivative spectrum concerning the analyte concentration, which reduces the effect of background but increases selectivity compared to the traditional methods [59].

In this research, we also employed one of the RSM methods, namely the Box-Behnken model (BBD), which is a response surface model more efficient than the three-level factorial or central composite designs. These designs include all general schemes using just three levels of factors that can be rotated partly or completely. While these designs lack combinations for complete components at their maximum and minimum values, BBD can decrease the number of necessary tests and prevent conducting studies under extreme situations that may result in unsatisfactory results [60].

However, a review of the literature indicates that CPE has only been implemented for eliminating solitary dyes. Given the presence of diverse dyes in real-world commercial effluents, evaluating the suggested procedures for the concurrent disposal of mixed dyes from water and wastewater is necessary [61]. In this investigation, first-order derivative spectrophotometry and the laboratory design were employed along with the CPE technique to concurrently eliminate CR and MO dyes. To this end, the effects of pH, electrolyte concentration, surfactant concentration, dye concentration, and cloud point temperature were investigated on the removal efficacy of the CPE system. Later, the characteristics of the solubilization isotherms and kinetic models of CR and MO were studied.

2. Experimental

2.1. Materials

The highest possible purity of CR, MO, phosphoric acid, sodium hydroxide, sodium chloride, and Triton X-100 were purchased from Merck Germany company. A stock solution containing 1000 mg/L of dyes was prepared in double-distilled water. The stock was first diluted to prepare the working standard solutions. A solution of phosphoric acid and a solution of sodium hydroxide were employed to prepare 0.1 M phosphate buffer solutions. A solution of 0.1M NaOH and phosphoric acid was utilized to modify the pH level using a pH meter.

2.2. Instruments

The UV–Vis spectrophotometer (model LUV 100A, Labnics, United States of America) was applied to measure the absorbance of CR and MO dyes. Wave scanning with UV software was performed at the 300–700 nm wavelength range and the wavelengths of 365 and 520 nm were selected for CR and MO dyes with the first-order derivative spectrum. A laboratory water bath was also employed to maintain the appropriate temperature.

2.3. Cloud point extraction process and dye analysis

In glass tapered tubes, 1.0 mL binary mixture of CR and MO dyes in aqueous solutions was prepared at a specific concentration, the Triton X-100 surfactant (0.11 mol/L), and NaCl (0.75 mol/L) at pH 5.7. Then, the mixture was heated in a bath of water at 70 °C for 35 min to produce segregation of the phases. In the following, the mixture was placed in an ice bath for 10 min so that the surfactant-rich phase got viscous and the final concentration of dye in the phase of dilute was determined using a UV–Vis spectrophotometer. The dye removal efficiency was calculated using Eq. (1):

$$\%Efficiency = \frac{C_{initial} - C_{dilute}}{C_{initial}} \times 100 \quad (1)$$

Where, $C_{initial}$ is the initial concentration of dye and C_{dilute} is the concentration of dye in the dilute phase. Therefore, an optimization process was performed by selecting the best laboratory conditions for dye removal [45].

The recovery studies [59] were recruited to verify the accuracy of the zero-crossing spectrophotometry method with a first-order derivative for evaluating the CR and MO dye concentrations in binary solutions. In this regard, two standard solutions were created including various concentrations of CR along with MO dyes. The concentration of MO was established at 5 mg/L in the first batch, while the CR content ranged from 1 to 50 mg/L. The same trend was utilized in the second batch to achieve standard MO solutions with concentrations within the range of 1–50 mg/L when there was 5 mg/L CR. Finally, synthetic combinations of varying concentrations of both dyes, ranging from 1 to 30 mg/L, were tested to demonstrate the validity of the suggested approach.

Equations (2) and (3) were used to calculate the relative errors (%) and recoveries (%) between calculated (Cc) and theoretical (Ct) concentrations [58].

$$Recovery\ (\%) = \frac{C_c}{C_t} \times 100 \quad (2)$$

$$Relative\ Error(\%) = \frac{C_c - C_t}{C_t} \quad (3)$$

2.4. Response surface methodology (RSM)

After selecting the appropriate ionic salt for extraction, RSM (a multivariate optimization method that finds the optimized conditions by performing the minimum number of tests) was used to optimize other factors, such as concentrations of CR, MO, surfactant, pH, temperature, and time. The design-Expert® software (version 10), which benefits from regression analysis, was also run for probationary design investigations. To assess the main effects of the study factors, 54 experiment runs were designed at random. The study factors, high and low levels, RSM matrix, and outcomes are demonstrated in Table 1. The second order polynomial as equation (4) can approximate the mathematical relationship between the six variables and the response:

$$Y = X_0 + X_1A + X_2B + X_3C + X_4D + X_5E + X_6F + X_{11}A^2 + X_{22}B^2 + X_{33}C^2 + X_{44}D^2 + X_{55}E^2 + X_{66}F^2 + X_{12}AB + X_{13}AC + X_{14}AD + X_{15}AE + X_{16}AF + X_{23}BC + X_{24}BD + X_{25}BE + X_{26}BF + \varepsilon \quad (4)$$

where X_0 is constant; X_1, X_2, X_3, X_4, X_5, X_6 are linear coefficients; X_{12}, X_{13}, X_{14}, X_{15}, X_{16}, X_{23}, X_{24} X_{25}, X_{26}, are cross-product coefficients; X_{11}, X_{22}, X_{33}, X_{44}, X_{55}, X_{66} are quadratic coefficients [62].

The statistical significance of the model equation and the goodness of fit of the model were evaluated by the coefficient

Table 1
Box-Behnken model design matrix.

Factors	Coded Variable (X!)	Experimental Field		
		−1	0	+1
A: Concentration of CR dye(mg/L)	X_1	1	75.5	150
B: Concentration of MO dye(mg/L)	X_2	1	75.5	150
C: Concentration of Triton X-100 (M)	X_3	0.01	0.07	0.12
D: pH	X_4	3	7	11
E: Temperature(°C)	X_5	40	70	100
F: Time(min)	X_6	5	32.5	60

determination (R^2) and by the F test analysis of variance (ANOVA). ANOVA is a statistical technique that subdivides the total variation in a set of data into component parts associated with specific sources of variation for the purpose of testing hypotheses on the parameters of the model. According to the ANOVA the large value of F indicates that most of the variation in the response can be explained by the regression equation. The associated P value is used to estimate whether F is large enough to indicate statistical significance.

3. Results and discussion

3.1. Dye analysis

The zero-order spectra of absorption were achieved for each dye within the wavelength range of 300–700 nm under optimal conditions. Wavelengths with maximum absorption levels of 435 and 480 nm were selected to study CR and MO in their single dye solutions at different concentrations. For CR and MO dyes, the calibration curves were linear within the range of 1–200 mg/L, although the correlation diverged at very high doses. According to the results of the optimization process for the target dyes, the optimal values were identical for the elimination of CR and MO. As a result, the simultaneous measurement of CR and MO in binary mixtures was performed at pH = 5.7, which allowed efficient removal of both dyes. A binary mixture containing 5 mg/L of each dye was provided for the simultaneous elimination of CR along with MO. Following the extraction of dyes using the suggested approach, the spectra of absorption with zero order were recorded (Fig. 1a).

The maximum wavelength of MO and CR in aqueous solution was as a single at 480 and 430 nm, but in the binary mixture of CR and MO from aqueous solutions, overlapping was obtained and direct measurement of absorbance using absorption spectra with zero order was not applicable for the simultaneous removal of the studied dyes. Consequently, the concurrent analysis of CR and MO dyes in

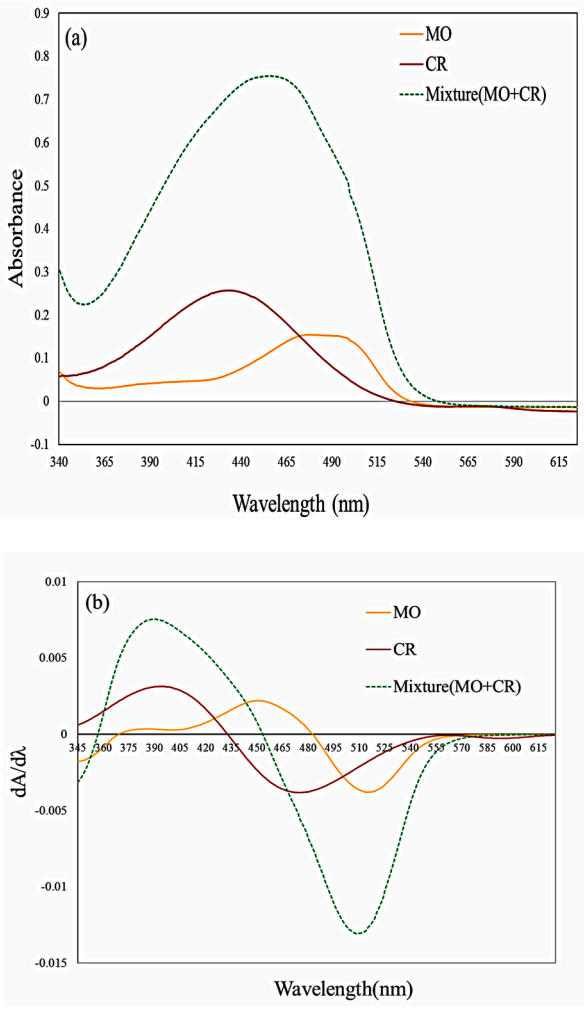

Fig. 1. Spectra of zero and first order derivatives of CR and MO dyes (initial dye concentration of 5mg/L).

mixtures of two substances was dependent on the examination of derivative absorption spectra. Fig. 1b illustrates the spectra of absorption with zero order of CR and MO in single and binary mixed solutions within the wavelength of 300–700 nm. Based on the measurement of the value of absorbance's first derivative of CR dye at 365 nm (1D365) when MO is present, where MO's derived absorbance was zero (zero crossing point), and at 520 nm (1D520) for MO dye in the presence of CR, where CR's derived absorbance was zero or close to zero value, simultaneous determination of CR and MO was performed with first derivative method.

According to Table 2 and based on the first-order derivative spectrophotometry, the recoveries increased from 94.3 to 99.5 % for CR and from 94.6 to 99.1 % for MO. In addition, the percentage error increased from 0.5 to 2.3 % for CR and from 0.6 to 3 % for MO, confirming the ability of derivative spectrophotometry to quantify the CR and MO concentrations in binary mixtures. This approach can eventually be used to detect other dye mixtures with overlapped spectra [58,63–67].

3.2. Optimization of ionic salts

In the elimination procedure, the optimization step is of great importance. In the present study, initially selected an ionic salt with a suitable concentration since salt promotes phase separation by increasing the movement of chemical constituents between different phases and declining the Cloud Point Temperature (CPT) [68]. When the temperature rises over the surfactant cloud point. It causes the micelles to lose water and the hydrophobic interactions between the micelles increase. If the surfactant concentration is high enough produce a cloudy solution, resulting in phase separation. The separation may occur at room temperature in the presence of specific salt, known as the salting-out phenomenon. The salting-out notion states that the solubility of a non-electrolyte decreases when there is a high concentration of electrolyte. The introduction of salt into a micellar solution enhances the hydrophobic contacts between micelles by increasing the dryness between them. When the surfactant concentration reaches a sufficient level, it leads to the formation of turbidity and enables phase separation. The use of the salting-out phenomena in CPE eliminates the need for heating and thereby decreases the duration of the separation process [61].

For this purpose, three ionic salts, namely Na_2SO_4, Na_2SO_3, and NaCl, were selected and compared for their ability to remove the dyes under study. According to the findings, NaCl had the highest elimination efficiency. When the concentration of this salt was optimized in the range of 0.25–1 mol/L, the 0.75 mol/L concentration showed the most effective results in removing dyes. According to Mortada et al. [61], salt can exacerbate the incompatibility between surfactant macromolecules and the structures of water in the hydration shells of the analytes. This can lower the concentration of "free water" in the surfactant-rich phase and decrease its volume consequently.

3.3. Box-behnken design

The other influencing factors were optimized using the RSM design. Table 3 shows the experimental results as well as a 6-factor BBD matrix for removing CR and MO. The model of quadratic was offered by the software and the experimental results were fitted accordingly, yielding regression equations (5) and (6) for the simultaneous removal of CR and MO dyes in a binary system:

$$\%E = 91.67 - 4.45X_1 - 3.67X_2 + 2.44X_3 - 1.67X_4 + 1.66X_5 + 0.79X_6 - 2.22X_1X_2 + 1.19X_1X_3 - 1.136X_1X_4 + 0.73X_1X_5 + 0.189X_1X_6 + 0.55X_2X_4 - 0.54X_2X_5 + 0.53X_2X_6 + 2.01X_3X_5 + 1.05X_3X_6 - 1.56X_4X_6 + 0.68X_5X_6 + 4.40X_1^2 - 1.28X_2^2 - 0.74X_3^2 - 0.59X_4^2 - 2.46X_5^2 - 1.33X_6^2 \quad (5)$$

$$\%E = 86.73 - 3.26X_1 - 6.64X_2 + 5.24X_3 - 15.59X_4 + 3.55X_5 - 1.80X_6 - 3.67X_1X_2 - 4.93X_1X_3 - 5.61X_1X_4 - 4.42X_1X_5 + 12.50X_1X_6 - 5.26X_2X_4 - 4.16X_3X_5 - 7.03X_3X_6 - 7.00X_4X_6 - 8.95X_2^2 - 7.38X_3^2 - 12.11X_4^2 - 4.28X_6^2 \quad (6)$$

Where, X_1, to X_6 are the independent variables.

In a sample, the percentage of CR and MO can be used to predict the removal effectiveness of each dye, revealing antagonistic and synergistic effects on removal performance [69]. The significance of the design coefficients was determined using the p-value factor.

The reliability and significance of Eqs. (5) and (6) were estimated using the Analysis of Variance (ANOVA) showing that the F

Table 2
First derivative spectrophotometric method used to measure CR and MO from aqueous solutions.

Sample	CR	MO	Regression equation for components	R^2	LOD(mg/L)
1	5	1–50	$\Delta A/_{\Delta\lambda} = -0.0007 - C_{MO}0.0004$	MO = 0.9914	MO = 0.4
2	1–50	5	$\Delta A/_{\Delta\lambda} = -0.0005 + C_{CR}0.0005$	CR = 0.992	CR = 0.3

Taken(mg/L)	Found (mg/L)		%Recovery		%Error	
	CR	MO	CR	MO	CR	MO
5	4.95	4.96	99.5	99.1	2	3
10	9.73	9.53	97.3	95.3	1.2	1.5
20	19.62	18.92	98.1	94.6	2.3	1
30	28.29	29.13	94.3	97.1	0.5	1.2
Average			97.3	96.53	1.5	1.68

Table 3
ANOVA data for the removal of CR and MO dyes from aqueous solutions.

Run Order	Factors						E% of CR		E% of MO	
	A	B	C	D	E	F	Observed	Predicted	Observed	Predicted
1	1	75.5	4.5	3	100	32.5	99.41	99.06	89.22	86.07
2	150	75.5	8	7	70	60	96.89	96.92	88.74	88.35
3	1	1	4.5	3	70	32.5	99.61	100.96	95.81	93.03
4	150	1	4.5	3	70	32.5	99.29	99.22	99.31	105.07
5	75.5	1	4.5	7	40	60	87.82	87.66	89.13	89.31
6	75.5	75.5	4.5	7	70	32.5	91.35	91.67	86.77	86.73
7	1	75.5	8	7	70	60	99.41	99.65	81.46	79.73
8	1	75.5	4.5	11	40	32.5	96.72	96.58	48.35	50.16
9	75.5	150	4.5	7	100	60	85.79	86.03	85.56	86.03
10	1	150	4.5	3	70	32.5	97.17	96.97	88.80	97.62
11	150	150	4.5	3	70	32.5	86.69	86.34	95.09	94.96
12	1	75.5	1	7	70	5	99.31	99.34	89.11	88.00
13	75.5	75.5	4.5	7	70	32.5	92.17	91.67	87.12	86.73
14	75.5	75.5	8	3	70	60	97.08	96.87	89.22	88.20
15	75.5	1	8	7	40	32.5	89.44	89.15	99.70	100.82
16	1	75.5	4.5	3	40	32.5	97.12	96.49	85.74	84.12
17	75.5	1	4.5	7	100	60	93.63	93.42	99.01	100.16
18	75.5	75.5	8	3	70	5	90.31	90.07	80.22	76.21
19	150	75.5	4.5	3	100	32.5	93.99	94.35	83.21	81.91
20	75.5	150	4.5	7	40	60	82.16	82.46	79.51	77.73
21	75.5	1	4.5	7	40	5	88.72	88.48	97.13	95.82
22	75.5	150	4.5	7	40	5	80.96	81.18	83.70	83.39
23	1	75.5	8	7	70	5	99.51	99.75	90.02	94.29
24	75.5	75.5	4.5	7	70	32.5	90.85	91.67	85.98	86.73
25	1	1	4.5	11	70	32.5	99.11	99.23	83.96	83.58
26	75.5	75.5	8	11	70	60	89.67	89.72	56.75	58.64
27	1	75.5	1	7	70	60	95.36	95.06	43.46	45.34
28	75.5	75.5	1	11	70	60	83.12	83.42	28.43	30.94
29	150	75.5	1	7	70	60	87.84	87.55	76.44	73.67
30	75.5	1	1	7	100	32.5	88.71	88.55	95.85	94.82
31	75.5	150	4.5	7	100	5	81.89	82.05	87.76	86.74
32	75.5	150	8	7	100	32.5	88.92	89.03	82.92	82.43
33	75.5	150	1	7	100	32.5	79.94	80.23	84.43	84.15
34	150	150	4.5	11	70	32.5	82.49	81.37	38.75	42.05
35	1	150	4.5	11	70	32.5	97.59	97.43	73.41	67.14
36	150	1	4.5	11	70	32.5	91.64	92.07	81.49	73.19
37	75.5	1	8	7	100	32.5	97.93	97.58	99.21	100.86
38	75.5	75.5	4.5	7	70	32.5	91.82	91.67	86.65	86.73
39	75.5	75.5	4.5	7	70	32.5	91.71	91.67	86.53	86.73
40	75.5	150	1	7	40	32.5	81.68	82.03	72.49	70.00
41	75.5	75.5	1	3	70	60	89.18	89.21	67.23	66.83
42	75.5	75.5	8	11	70	5	89.14	89.17	50.83	49.74
43	75.5	150	8	7	40	32.5	82.61	82.78	84.73	84.93
44	75.5	1	4.5	7	100	5	91.83	91.53	99.10	101.71
45	150	75.5	4.5	11	40	32.5	83.39	83.51	38.63	41.27
46	150	75.5	4.5	11	100	32.5	87.16	87.56	52.41	53.51
47	150	75.5	1	7	70	5	84.47	84.29	66.09	66.33
48	150	75.5	4.5	3	40	32.5	88.42	88.84	97.43	97.66
49	150	75.5	8	7	70	5	89.22	89.47	53.28	52.90
50	75.5	75.5	1	11	70	5	86.89	87.05	47.62	50.14
51	75.5	1	1	7	40	32.5	88.27	88.17	76.79	78.12
52	75.5	75.5	1	3	70	5	86.71	86.60	83.34	82.95
53	75.5	75.5	4.5	7	70	32.5	92.12	91.67	87.33	86.73
54	1	75.5	4.5	11	100	32.5	97.89	97.70	79.82	80.10

Source	Df	CR dye				MO dye			
		SS	MS	F-Value	p-value	SS	MS	F-Value	p-value
Model	27	1776.31	65.79	233.79	<0.0001	16653.95	616.81	44.37	<0.0001
A	1	474.55	474.55	1686.34	<0.0001	255.39	255.39	18.37	0.0002
B	1	323.47	323.47	1149.49	<0.0001	1057.88	1057.88	76.09	<0.0001
C	1	143.33	143.33	509.32	<0.0001	659.40	659.40	47.43	<0.0001
D	1	67.23	67.23	238.92	<0.0001	5833.47	5833.47	419.58	<0.0001
E	1	65.94	65.94	234.31	<0.0001	302.25	302.25	21.74	<0.0001
F	1	15.03	15.03	53.40	<0.0001	77.98	77.98	5.61	0.0256
AB	1	39.56	39.56	140.58	<0.0001	108.04	108.04	7.77	0.0098
AC	1	11.40	11.40	40.51	<0.0001	194.24	194.24	13.97	0.0009

(*continued on next page*)

Table 3 (*continued*)

Source	Df	CR dye				MO dye			
		SS	MS	F-Value	p-value	SS	MS	F-Value	p-value
AD	1	29.46	29.46	104.68	<0.0001	503.22	503.22	36.19	<0.0001
AE	1	4.32	4.32	15.36	0.0006	156.56	156.56	11.26	0.0024
AF	1	28.46	28.46	101.15	<0.0001	1250.50	1250.50	89.94	<0.0001
BD	1	2.39	2.39	8.48	0.0073	221.13	221.13	15.91	0.0005
CE	1	32.40	32.40	115.14	<0.0001	138.61	138.61	9.97	0.0040
CF	1	17.54	17.54	62.31	<0.0001	789.89	789.89	56.81	<0.0001
B^2	1	16.81	16.81	59.73	<0.0001	823.25	823.25	59.21	<0.0001
C^2	1	5.63	5.63	19.99	0.0001	560.44	560.44	40.31	<0.0001
D^2	1	3.59	3.59	12.76	0.0014	1508.28	1508.28	108.49	<0.0001
F^2	1	18.11	18.11	64.37	<0.0001	188.77	188.77	13.58	0.0011
Residual	26	7.32	0.28			361.48	13.90		
Lack of Fit	21	6.07	0.29	1.15	0.4802	360.36	17.16	76.43	<0.0001
Pure Error	5	1.25	0.25			1.12	0.22		
Cor Total	53	1783.62				17015.43			
R-Squared				0.9959				0.9788	
Adj-R-Squared				0.9916				0.9567	
Pred-R-Squared				0.9812				0.8893	
Adequate Precision				54.252				27.609	

values for CR and MO are 233.79 and 44.37, respectively (Table 3). These values indicate the significance of the proposed model for removing these two dyes from the existing process. On the other hand, extremely low p-values ($\leq$0.05) for the dyes in the quadratic equation indicate statistical significance [34,70,71]. These values were offered at a remarkably significant level for both models. According to the data in Table 3, the B, C, D, E, F, AB, AC, AD, AE, AF, BD, BE, BF, CE, CF, DF, EF, A^2, B^2, C^2, D^2, E^2, F^2 for CR along with A, B, C, D, E, F, AB, AC, AD, AE, AF, BD, CE, CF, DE, B^2, C^2, D^2, F^2 for MO coefficients were significant with minimal P-values ($P < 0.05$) while the other coefficients were non-significant ($P > 0.05$). In this analysis, R^2 (determination coefficient) values were respectively obtained as 0.9959 and 0.9788 for CR and MO, which are well balanced by the experimental data since all deviations were justified via the regression design [72,73]. The R^2 adjusted determination coefficient values (R^2 adj) tended to be 0.9916 and 0.9567 for CR and MO, respectively. The values of R^2 adj and R^2 were extremely close to each other, which is similar to the literature [74]. The R^2 pred values were respectively 0.9992 and 0.9983 for CR and MO matching with the R^2 adj value and reasonably consistent with the correlation values. In addition, the coefficient of variation (CV) for CR was equal to 0.58 percent for CR and 4.73 percent for MO, confirming the trustworthiness of this model as reported by the literature [28]. Fig. 2a and b indicate the normal probability vs externally studentized residuals so that the points should be in a roughly straight line in a normal distribution. Given that the points in Fig. 2a and 2b illustrate a straight line, they are presumed to be regularly distributed [35]. The residuals' normal distributions indicate the veracity of the assumptions and the residuals' independence [75]. Fig. 2c and d demonstrate the relationship between the actual and projected values for the dye removal. The anticipated and actual positions were typically close to each other (Fig. 2c and d). This finding corroborates the research's experimental findings [76,77].

Fig. 3(a–c) display the contour plots for concentration of Triton X-100, pH, and temperature variables for both dyes. According to the interpretation of the graphs, the concentration of the surfactant Triton X-100 (investigated between 0.01 and 0.12 mol/L) has a direct effect on elimination performance. The model for Triton X-100 presents a concentration of 0.11 mol/L as the optimal value. These dyes cannot be removed with substantial efficiency at low surfactant concentrations so that a rise in the concentration of surfactant higher than this range would not result in a significant increase in dye removal outcome. The real number of micelles grow as the surfactant concentration rises, improving the dye molecule solubility as a result [78]. In this process, the optimal amounts for removing CR and MO dyes were respectively determined as 11.24 and 13.52 mg/L, indicating the restricted adsorption ability of the surfactant as an adsorbent, which prevented further removal. The antagonistic impact of each dye is detectable at adsorption, which results in a decreased adsorption yield [59].

Considering the critical role of pH in the efficiency of dye removal, the role of pH in dye removal was surveyed in the range of pH = 3–11 and a pH equal to 5.77 was considered as optimal. The dye adsorption capability was determined utilizing the strength of the ionic interaction between the adsorbent and the dyes [79]. Typically, the absorption capacity will be high when cationic dyes are at basic pH and anionic dyes are usually adsorbed on the adsorbent surface at acidic pH, which is the interaction of strong electrostatics between opposite charges that molecules of dye and their residue create over the adsorbent surface [79,80].

The final variables to be optimized were temperature and time. For this purpose, the temperature was set within the range of 40 °C and 100 °C, and the time was between 5 and 60 min. The optimized temperature and time were respectively 70.8 °C and 35.96 min based on the RSM results. Non-ionic surfactants became more hydrophobic at higher temperatures because of an equilibrium shift that favors dehydration with ether oxygen [81]. With an increase in temperature, the critical micelle concentration (CMC) of non-ionic surfactants diminished [82]. As temperature rises, the number of micelles and their ability to dissolve substances in the solution increased, resulting in a greater ability to remove dyes. However, at temperatures higher than 70 °C, the system reversed and reduced the efficiency of removal.

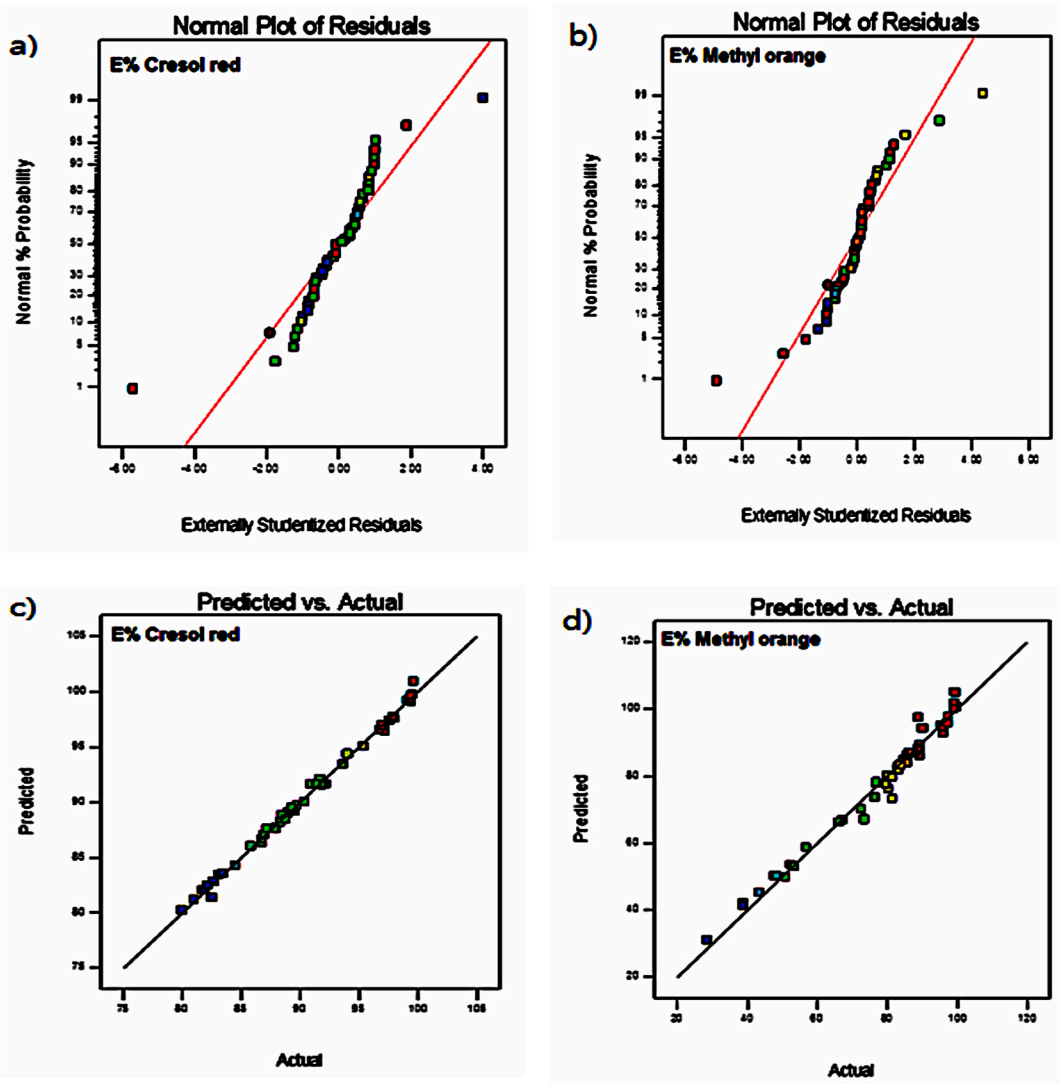

Fig. 2. The plots of normal probability of the residuals for co-elimination of CR (a) and MO (b) dyes and predicted values versus experimental data for co-elimination of CR (c) and MO (b) dyes.

3.4. Kinetic models

The process of adsorption can be explained through several kinetic models, consisting of the pseudo-first order [83], pseudo-second order [84], and intraparticle diffusion models, to assess the dynamical empirical data, as shown in nonlinear Eqs. (7) and (8), respectively.

$$q_t = q_e\left(1 - \exp^{-k_1 t}\right) \tag{7}$$

$$q_t = \frac{q_e^2 k_2 t}{1 + q_e k_2 t} \tag{8}$$

Where, q_t represents the absorbed amount of dyes per unit mass on adsorbent at any time t (mg/g), q_e represents the quantity of each dye's equilibrium adsorption per unit mass (mg/g), k_1(1/min), and k_2(g/mg min) demonstrates the constants for the pseudo-first-order and pseudo-second-order models, respectively. The model of pseudo–first-order, proffered by Lagergren in 1898, assumes that the rate of solute uptake changes proportionally to the difference between the saturation concentration and the amount of solid uptake as time passes. This model is typically valid during the initial stage of the adsorption procedure. The pseudo–second-order kinetic model is based on the assumption that the rate-limiting step is either chemical sorption or chemisorption. It provides predictions for the whole spectrum of the adsorption behavior. The adsorption rate in this situation is specified by the adsorption capacity rather than the

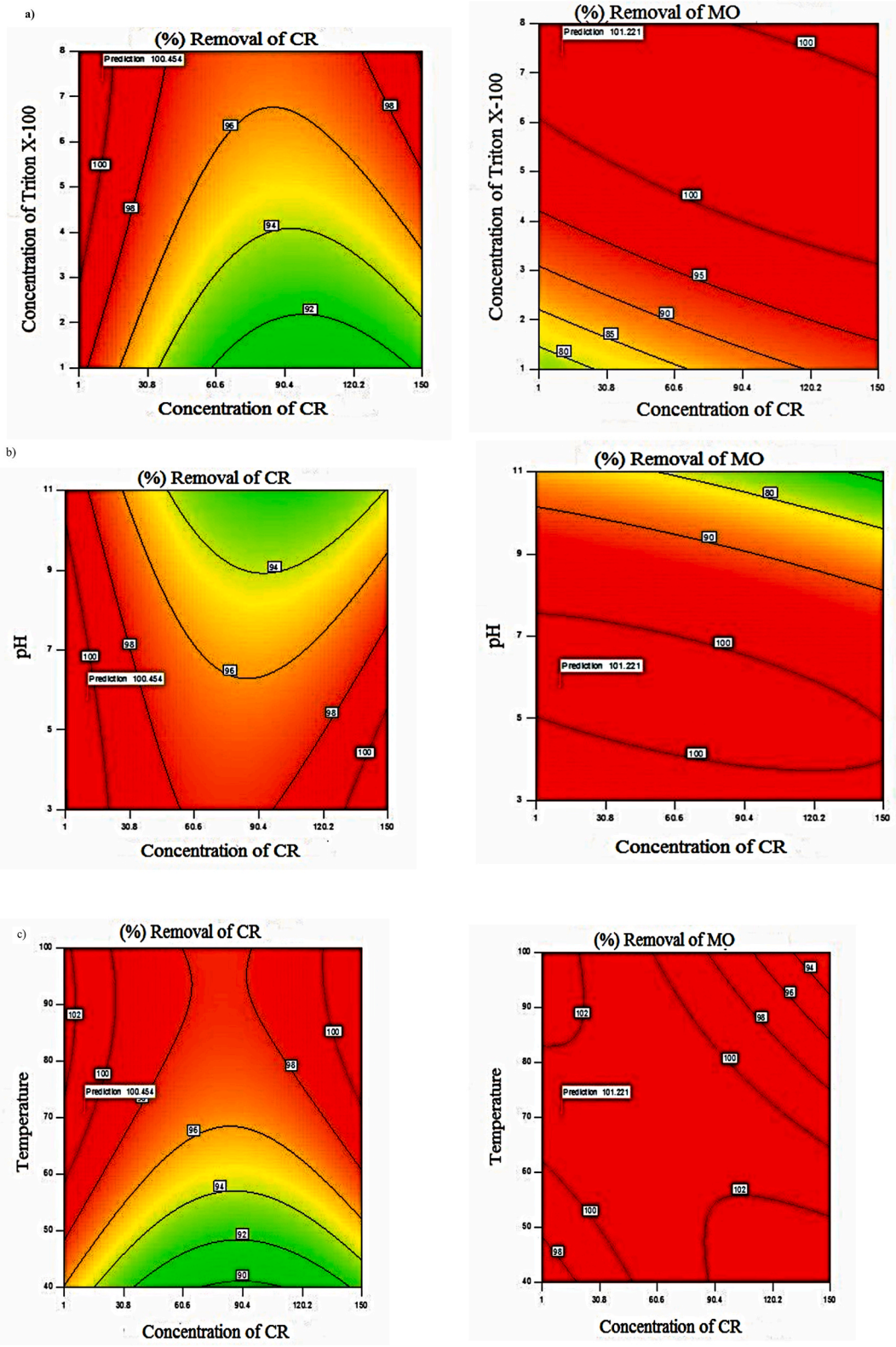

Fig. 3. Contour plots for (a) surfactant concentration, (b) pH and (c) temperature for CR and MO dyes from aqueous solutions.

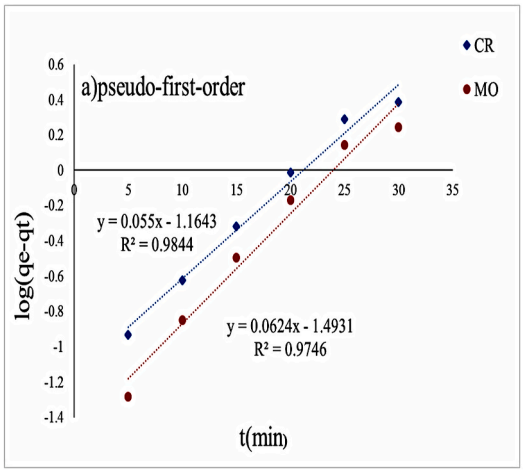

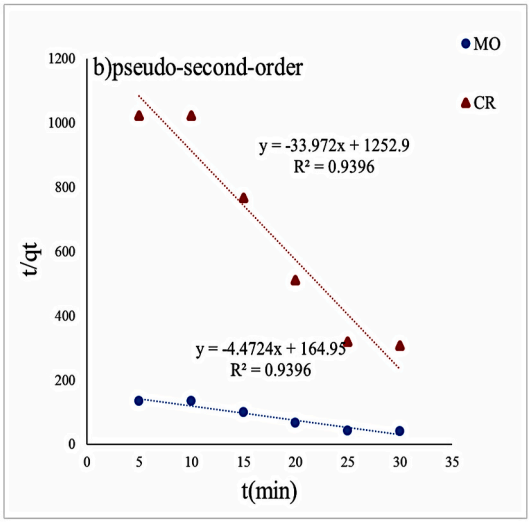

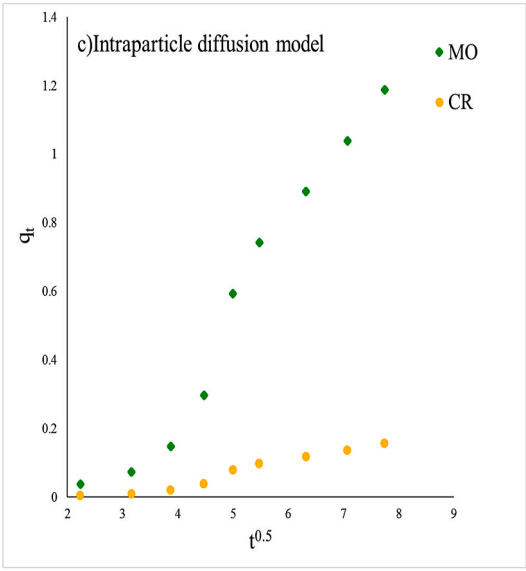

Fig. 4. Adsorption kinetic models (a) pseudo-first order kinetic model, (b) pseudo-second order kinetic model and (c) intraparticle diffusion model for adsorption of CR and MO dyes onto Triton X-100.

concentration of the substance being adsorbed [84,85]. The data collected from the pseudo-first-order and the pseudo-second-order models of kinetic are depicted in Fig. 4a and b. When compared to pseudo-second-order, the numbers for the pseudo-first-order's coefficient of determination (R^2) are significantly greater. The pseudo-first-order model demonstrated a determination coefficient (R^2) value of higher than 0.97, surpassing the R^2 value of 0.93 obtained from the pseudo-second-order model for the two investigated dyes. The determination coefficient values indicate that the kinetic pseudo-first-order model is the most appropriate for describing the data and the adsorption mechanisms involving Triton X-100 and both dyes properly. Furthermore, the amounts of adsorption calculated by the pseudo-first-order model in equilibrium closely resemble those found experimentally [86].

According to Marco-Brown et al. [87], the intraparticle diffusion model may be characterized as equation (9) follows:

$$q_t = k_p t^{0.5} + C \tag{9}$$

In the given context, "qt" represents the amount of CR and MO dyes adsorbed at a certain time "t". Where, "kp" (mg/g $min^{-0.5}$) indicates the rate constant of intraparticle diffusion. "C" refers to the constant calculated from the intercept of the equation when plotting "qt" against "$t^{0.5}$". The adsorption of CR along with MO dye molecules may be divided into three distinct phases, as seen in Fig. 4c. The first step involves quick adsorption on the outer surface and the second phase is characterized by slow adsorption. In the third phase, equilibrium is reached due to the reduced concentration of dye in the liquid phase and the absence of accessible active sites. The values of the intraparticle diffusion parameters (kp and C) as well as the regression determination coefficient (R^2) for CR and MO were 0.04, 0.32, 0.14, 1.1, and 0.98, respectively. The high R^2 values indicate that the intraparticle diffusion model represents the adsorption process appropriately. Despite the linear correlation, none of the graphs intersected at the origin due to the disparity in mass transfer rate between the first and final adsorption phases. In addition, the non-zero intercepts of these plots illustrated that intraparticle diffusion did not serve as the only rate-controlling step in the process of adsorption of CR along with MO dyes by the created adsorbent Triton X-100 [39].

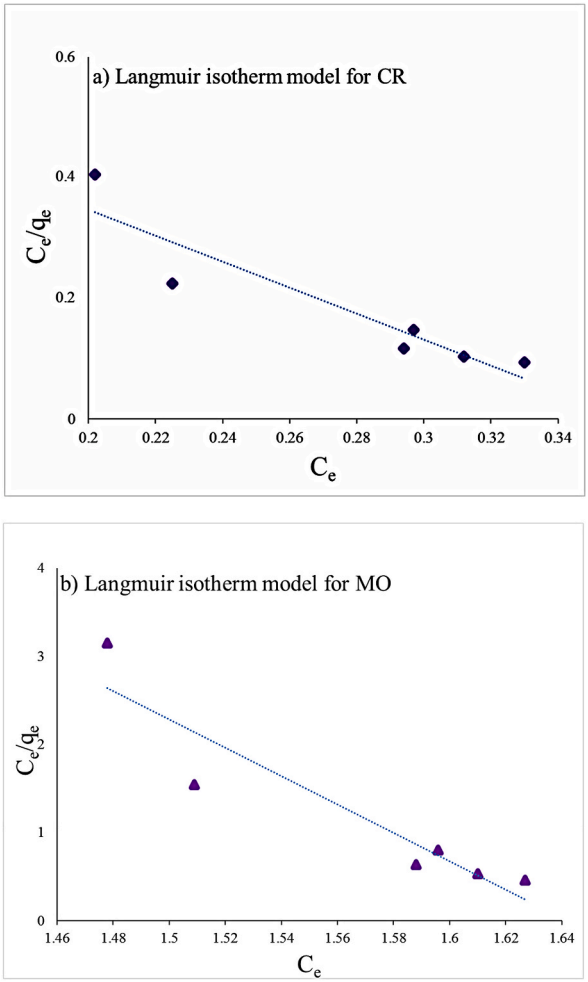

Fig. 5. Isotherm of solubilization a) CR and b) MO dyes on Triton X-100 surfactant.

3.5. Isotherms models of adsorption

The models' objective is to examine the process of interaction by extracting the surfactant Triton X-100 and impurities of CR and MO dyes to determine the most efficient, appropriate, and cost-effective surfactant. In this regard, CPE stands for the potential for interaction between a contaminating species and surfactant micelles. This interaction may be interpreted as a sorption procedure in which species with contaminating (adsorbate) attach to the surface of micelles of surfactant (adsorbent) like Triton X-100 or other positions inside the micelles. In this scenario, Triton X-100 micelles serve as a highly responsive center readily available for sorption. Triton X-100 micelles can sequester contaminating species, such as CR and MO dyes, inside their cores or outside layers. This phenomenon may be seen by examining the monolayer sorption on the micelles' surface. Hence, the sorption process can be described using the Langmuir isotherm mathematical model [88]. The isotherm of the Langmuir model is mostly applied by multiple scholars and may be mathematically represented by equations (10) and (11) [88].:

$$q_e = Q_{max}\frac{bC_e}{1 + bC_e} \tag{10}$$

$$\frac{C_e}{q_e} = \frac{1}{bQ_{max}} + \frac{1}{Q_{max}} \times C_e \tag{11}$$

The variable q_e represents the quantity of CR along with MO dyes absorbed or dissolved per mole of Triton X-100 at equilibrium (in moles per mole). Ce represents the concentration of equilibrium of CR along with MO dyes in the micellar-dilute phase (in moles per liter). The solubilization capacity or monolayer capacity (Qmax) is a measure of the amount of solute that can be dissolved per unit of solvent (mol/mol). The energy necessary to dissolve CR and MO dye species (L/mol) is demonstrated by the constant b [89]. The model has been applied to associate the equilibrium data for solubilization of CR and MO dye species across all concentrations (Fig. 5a and b). The plot of Ce/qe against Ce illustrates a linear relationship between CR and MO dyes that were either solubilized or sorbed onto Triton X-100 micelles (Fig. 5a and b). This confirms accurate description of the solubilization isotherm by this term. The Qmax and (b) values were determined by analyzing the intercept and slope of the linear graph depicting Ce/qe against Ce. The capacity of sorption (Qmax) and the sorption heat (b) are two indicators that demonstrate the sorption ability of Triton X-100 micelle. The temperature is a differentiating factor for Triton X-100, CR, and MO in CPE system, causing Qmax and (b) to vary. As previously stated by Nsour and Rawajfih [90], sorption follows the Langmuir model when the correlation coefficient value, R^2, exceeds 0.8. The R^2 values found in our system, specifically for the Triton X-100 - CR and MO dyes, are represented in Table 4. The values above 0.8 indicate that the isotherm was in accordance with the model of Langmuir [89]. The sorption isotherm of CR and MO dyes followed the Langmuir model, indicating a mechanism of monolayer coverage. maximum adsorption capacities, Q_{max} (mol/mol), quantifies the adsorbent's (micelles) ability to hold the adsorbed solute effectively (CR and MO dyes). This suggests that Triton X-100 can be effective as an extractant or sorbent for CR and MO dyes. The Langmuir model is distinguished by the separation factor (RL), which can be obtained from equation (12) described by Hamed et al. [91,92].

$$R_L = \frac{1}{1 + bC_0} \tag{12}$$

The RL value determines the nature of the isotherm pattern, demonstrating whether it is irretrievable ($RL = 0$), favorable ($0 < RL < 1$), linear ($RL = 1$), or unfavorable ($RL > 1$). The retention factor (RL) for this system was determined to be less than 1 and greater than 0, demonstrating the advantageous sorption of CR along with MO dyes onto the micelles of Triton X-100 [93]. Equation number 9 and the determined parameters of Qmax and (b) can be used to determine the necessary quantity of Triton X-100 for eliminating CR and MO dyes by CPE to achieve the desired level [85]. From the Langmuir isotherm model, the maximum adsorption capacities of Triton X-100 were determined to be 0.77 mol/mol for CR and 26.41 mol/mol for MO. Table 6 shows the results of the comparison Qmax of the CR and MO dyes with other adsorbents. As can be seen, the Triton X-100 has a good Qmax for both CR and MO dyes and is competitive with other reported adsorbents in terms of performance [94–105].

3.6. Thermodynamics of the extractive elimination proceeding

The thermodynamic variables are essential in practical applications of pollution removal processes since they allows for assessing the capability and spontaneity of the treatment procedure [106]. The hydrophobicity of non-ionic surface-active agents, such as Triton X-100, increases at higher temperatures due to the enhanced dehydration of the ether oxygen. Consequently, a substantial increase was observed in the concentration of micelles formed by Triton X-100. The solubility of micelles will increase at higher temperatures resulting in an enhanced removal process of CR and MO dyes [88,91,92]. The thermodynamic functions, such as Gibbs-free-energy (ΔG°), enthalpy (ΔH°), and entropy (ΔS°) were calculated using the methodology described by Melo et al. with equations (13)–

Table 4
Isotherm parameters for the adsorption of CR and MO dyes on Triton X-100.

Species	Q_{max}(mol/mol)	R_L	b(L/mol)	R^2
CR	0.77	0.08	2.14	0.86
MO	26.41	0.01	16.08	0.87

(16) [85]:

$$\Delta G^{\circ} = -2.303RT\log K_C \tag{13}$$

$$\Delta G^{o} = \Delta H^{o} - T\Delta S^{o} \tag{14}$$

$$-2.303RT\log Kc = \Delta H^{o} - T\Delta S^{o} \tag{15}$$

$$\log K_C = \log\left(\frac{q_e}{C_e}\right) = \frac{\Delta S^{o}}{2.303R} + \frac{-\Delta H^{o}}{2.303R}\frac{1}{T} \tag{16}$$

$$q_e = \frac{\text{Moles of CR and MO dyes solubilized}}{\text{Moles of Triton X} - 100 \text{ used}} = \frac{V_o C_o - V_d C_e}{C_s V_o} \tag{17}$$

The variable qe in equation (17) represents the quantity of CR along with MO dyes that are either absorbed or dissolved per mole of Triton X-100 at equilibrium, measured in moles per mole. Ce represents the concentration of equilibrium of CR along with MO dyes in the micellar-dilute phase, measured in milligrams per liter. Kc is used to describe the affinity for solubilization. Vo along with Vd represents the volumes of the CR along with MO dye solution, as well as the phase of aqueous, before and behind the CPE proceeding. The values of ΔH° and ΔS° are obtained by plotting logKc versus 1/T, as shown in equation (16). Fig. 6 depicts a linear relationship between the changes in enthalpy and entropy by analyzing the slope along with the intercept. Table 5 indicates the values derived from this diagram. The negative values of ΔG° indicate that the solubilization (removal) of CR and MO dyes is thermodynamically favorable and can occur spontaneously. The rise in the ΔG° negative values together with temperature provides the greatest driving force for the solubilization of CR and MO dyes, resulting in a better dye elimination as the operating temperature increases. The positive change in enthalpy (ΔH°) implies that the process of removing or solubilizing CR and MO dyes is thermodynamically favorable requiring heat input. The endothermic character of this phenomenon is also associated with the enhanced extraction or dissolution of CR and MO dyes as the temperature rises [85,93]. In addition, a positive change in entropy (ΔS°) corresponds to a reduction in the number of possible configurations of the adsorbed CR and MO dyes. This indicates a strong attraction between CR and MO dyes and Triton X-100 [85].

4. Limitations

The restrictions of CPE are primarily due to the complex nature of surfactants, restricting the discovery of analytes. Additionally, there are challenges in extracting certain substances that require creating a micellar system. Non-ionic surfactants have lower efficiency in extracting polar molecules and the stage separation process is limited by temperature when extracting thermally labile components. Furthermore, additional treatment of certain extracts may be necessary before measurement since there are difficulties in automating the CPE process [54].

5. Conclusion

In the present research, CPE coupled with derivative spectrophotometry were applied to eliminate anionic dyes, such as CR and MO from an aqueous solution. Box-Behnken model, an RSM-based method design of experiment, was employed to optimize the elimination conditions. The quadratic model was suggested by ANOVA of RSM data and coefficients of determination (R^2) $\geq$0.97 were obtained. The efficiency of dye extraction was enhanced by increasing the time, temperature, surfactant concentration, and salt concentration. The most effective factor in removing dyes was the dye concentration but the least important factor was time. The results indicated that the adsorption of these dyes could be accurately described using the pseudo-first-order model and this model demonstrated a

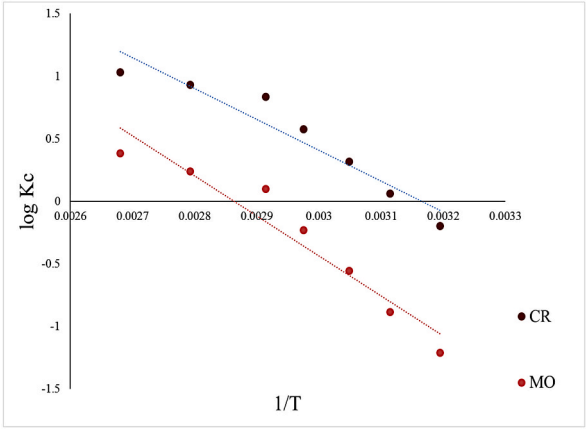

Fig. 6. Van't Hoff plot of removal of CR and MO dyes by CPE.

Table 5
Thermodynamic parameters for the removal of CR and MO dyes from aqueous solutions.

Temp.(K)	ΔH°(KJ/mol)		ΔS°(KJ/mol)		ΔG°(KJ/mol)	
	CR	MO	CR	MO	CR	MO
336					−156.81	−57.39
343	831.06	1215	3.25	3.61	−211.52	−80.1
358					−328.75	−121.56
373					−445.98	−217.59

Table 6
Comparison of the maximum adsorption capacity of CR and MO onto different adsorbents.

No	Adsorbent	dye	Q_{max}	References
1	Albizzia lebbeck seed activated carbon	CR	5.154 mg/g	[94]
2	Magnetic Fe_3O_4/C core–shell nanoparticles	CR	11.22	[95]
3	Sistan sand	CR	0.120 mg/g	[96]
4	Polypyrrole-decorated bentonite magnetic nanocomposite (MBnPPy)	MO	98.04 mg/g	[97]
5	Magnetic biochar (MBC)	MO	437.18 mg·/g	[98]
6	Magnetic Ni@C nanoadsorbents	MO	32 mg·/g	[99]
7	UiO-66-NS	MO	242/72 mg·/g	[100]
8	MnO_2@LNPs	MO	227 mg·/g	[101]
9	Hexagonal zinc oxide	MO	80.39 mg·/g	[102]
10	Chitosan/tannin/montmorillonite (Cs/Tn/MMT) films	MO	57.37 mg/g	[103]
11	Mesoporous carbon-silica composite (MMCS)	MO	113.1 mg/g	[104]
12	Polyaniline-coated kapok (Ceiba pentandra) fibers	MO	75.76 mg/g	[105]
13	Triton X-100	MO and CR	0.77 mol/mol for CR and 26.41 for MO	This work

determination coefficient (R^2) value of higher than 0.97. Furthermore, the sorption of CR and MO onto micelles of Triton X-100 can be effectively modeled using the Langmuir model. An increase in entropy (ΔS°) suggests that the solubilized CR and MO molecules are arranged in a more disordered way inside the micellar-rich phase. The findings showed that this method is simple, fast, economical, exact, and effective. Accordingly, derivative spectrophotometry along with CPE strategies are suggested to be employed in eliminating the binary mixture of chemical dyes. Since this approach is economically efficient, it may be referred to as a zero-waste strategy. The surfactant may be recovered and reused in the removal process by adding an appropriate solvent.

CRediT authorship contribution statement

Shahnaz Sargazi: Writing – original draft, Methodology, Investigation, Formal analysis, Data curation, Conceptualization. **Mohammad Taghi Ghaneian:** Writing – review & editing, Conceptualization. **Mashaallah Rahmani:** Writing – review & editing, Software, Project administration, Methodology, Data curation, Conceptualization. **Ali Asghar Ebrahimi:** Writing – review & editing, Conceptualization.

Compliance with ethical standards

This article does not contain any studies involving human or animal subjects.

Data availability

Data will be made available on request.

Declaration of competing interest

The authors declare that they have no known competing financial interests or personal relationships that could have appeared to influence the work reported in this paper.

Acknowledgments

This research was supported by Shahid Sadoughi University of Medical Sciences, Iran: Yazd and Zahedan University of Medical Sciences, Iran.

References

[1] S. Wong, N.A. Ghafar, N. Ngadi, F.A. Razmi, I.M. Inuwa, R. Mat, N.A.S. Amin, Effective removal of anionic textile dyes using adsorbent synthesized from coffee waste, Sci. Rep. 10 (2020) 2928.
[2] H. Farhadi, N. Keramati, Investigation of kinetics, isotherms, thermodynamics and photocatalytic regeneration of exfoliated graphitic carbon nitride/zeolite as dye adsorbent, Sci. Rep. 13 (2023) 14098.
[3] R.W. Jadhav, D.D. La, V.G. More, H. Tung Vo, D.A. Nguyen, D.L. Tran, S. V Bhosale, Self-assembled kanamycin antibiotic-inorganic microflowers and their application as a photocatalyst for the removal of organic dyes, Sci. Rep. 10 (2020) 154.
[4] M.M.H. Elzahar, M. Bassyouni, Removal of direct dyes from wastewater using chitosan and polyacrylamide blends, Sci. Rep. 13 (2023) 15750.
[5] J.B. Adeoye, D.O. Balogun, O.J. Etemire, P.N. Ezeh, Y.H. Tan, N.M. Mubarak, Rapid adsorptive removal of eosin yellow and methyl orange using zeolite Y, Sci. Rep. 13 (2023) 21373.
[6] K. Valizadeh, A. Bateni, N. Sojoodi, M.R. Ataabadi, A.H. Behroozi, A. Maleki, Z. You, Magnetized inulin by Fe3O4 as a bio-nano adsorbent for treating water contaminated with methyl orange and crystal violet dyes, Sci. Rep. 12 (2022) 22034.
[7] Occupational Safety and Health Standards, Hazard Communication., Toxic Hazard. Subst. (n.d.). https://www.osha.gov/laws-regs/regulations/standardnumber/1910/1910.1200.
[8] H. Trabelsi, M. Khadhraoui, O. Hentati, M. Ksibi, Titanium dioxide mediated photo-degradation of methyl orange by ultraviolet light, Toxicol. Environ. Chem. 95 (2013) 543–558.
[9] Y. Tang, M. Li, C. Mu, J. Zhou, B. Shi, Ultrafast and efficient removal of anionic dyes from wastewater by polyethyleneimine-modified silica nanoparticles, Chemosphere 229 (2019) 570–579.
[10] N.B. Singh, G. Nagpal, S. Agrawal, Water purification by using adsorbents: a review, Environ. Technol. Innov. 11 (2018) 187–240.
[11] M.S. Tehrani, R. Zare-Dorabei, Competitive removal of hazardous dyes from aqueous solution by MIL-68 (Al): derivative spectrophotometric method and response surface methodology approach, Spectrochim. Acta Part A Mol. Biomol. Spectrosc. 160 (2016) 8–18.
[12] A. Loqman, B. El Bali, A. El Gaidoumi, A. Boularbah, A. Kherbeche, J. Lützenkirchen, The first application of moroccan perlite as industrial dyes removal, Silicon (2021) 1–26.
[13] M.S. Tehrani, R. Zare-Dorabei, Highly efficient simultaneous ultrasonic-assisted adsorption of methylene blue and rhodamine B onto metal organic framework MIL-68 (Al): central composite design optimization, RSC Adv. 6 (2016) 27416–27425.
[14] F. Ramezani, R. Zare-Dorabei, Simultaneous ultrasonic-assisted removal of malachite green and methylene blue from aqueous solution by Zr-SBA-15, Polyhedron 166 (2019) 153–161.
[15] Y. Yao, S. Miao, S. Liu, L.P. Ma, H. Sun, S. Wang, Synthesis, characterization, and adsorption properties of magnetic Fe3O4@ graphene nanocomposite, Chem. Eng. J. 184 (2012) 326–332.
[16] A. Kiani, P. Haratipour, M. Ahmadi, R. Zare-Dorabei, A. Mahmoodi, Efficient removal of some anionic dyes from aqueous solution using a polymer-coated magnetic nano-adsorbent, J. Water Supply Res. Technol. 66 (2017) 239–248.
[17] A. Aichour, H. Zaghouane-Boudiaf, H.D. Khodja, Highly removal of anionic dye from aqueous medium using a promising biochar derived from date palm petioles: characterization, adsorption properties and reuse studies, Arab. J. Chem. 15 (2022) 103542.
[18] H. Chen, J. Zhao, J. Wu, G. Dai, Isotherm, thermodynamic, kinetics and adsorption mechanism studies of methyl orange by surfactant modified silkworm exuviae, J. Hazard Mater. 192 (2011) 246–254.
[19] S. Srinivasan, R.S. Kaarmukhilnilavan, K. Murugesan, Removal of malachite green using carbonized material derived from disposable facemasks: optimization of removal process through box-behnken design, Environ. Technol. (2023) 1–28.
[20] A. Dra, K. Tanji, A. Arrahli, A. El Gaidoumi, A. Kherchafi, A.C. Benabdallah, A. Kherbeche, Corrigendum to "Valorization of oued sebou natural sediments (Fez-Morocco Area) as adsorbent of methylene blue dye: kinetic and thermodynamic study,", Sci. World J. 2020 (2020).
[21] W. Jin, Y. Zhang, Sustainable electrochemical extraction of metal resources from waste streams: from removal to recovery, ACS Sustain. Chem. Eng. 8 (2020) 4693–4707.
[22] R. Khanpour, M.R. Sheikhi-Kouhsar, F. Esmaeilzadeh, D. Mowla, Removal of contaminants from polluted drilling mud using supercritical carbon dioxide extraction, J. Supercrit. Fluids 88 (2014) 1–7.
[23] R. Guedes-Alonso, Z. Sosa-Ferrera, J.J. Santana-Rodríguez, An on-line solid phase extraction method coupled with UHPLC-MS/MS for the determination of steroid hormone compounds in treated water samples from waste water treatment plants, Anal. Methods 7 (2015) 5996–6005.
[24] A. Szyguła, E. Guibal, M.A. Palacín, M. Ruiz, A.M. Sastre, Removal of an anionic dye (Acid Blue 92) by coagulation–flocculation using chitosan, J. Environ. Manage. 90 (2009) 2979–2986.
[25] A. Matilainen, M. Vepsäläinen, M. Sillanpää, Natural organic matter removal by coagulation during drinking water treatment: a review, Adv. Colloid Interface Sci. 159 (2010) 189–197.
[26] H. Cui, X. Huang, Z. Yu, P. Chen, X. Cao, Application progress of enhanced coagulation in water treatment, RSC Adv. 10 (2020) 20231–20244.
[27] S. Kashefi, S.M. Borghei, N.M. Mahmoodi, Covalently immobilized laccase onto graphene oxide nanosheets: preparation, characterization, and biodegradation of azo dyes in colored wastewater, J. Mol. Liq. 276 (2019) 153–162.
[28] S. Sekar, M. Surianarayanan, V. Ranganathan, D.R. MacFarlane, A.B. Mandal, Choline-based ionic liquids-enhanced biodegradation of azo dyes, Environ. Sci. Technol. 46 (2012) 4902–4908.
[29] G. Panthi, M. Park, H.-Y. Kim, S.-Y. Lee, S.-J. Park, Electrospun ZnO hybrid nanofibers for photodegradation of wastewater containing organic dyes: a review, J. Ind. Eng. Chem. 21 (2015) 26–35.
[30] L. Mardi, K. Tanji, A. El Gaidoumi, Y. Fahoul, I. El Mrabet, A. Arrahli, C. Chadli, L. Nahali, B. El Fathi, O. Boualam, Catalytic wet oxidation degradation of malachite green with Cu-coated sediment as catalyst: parameter optimization using response surface methodology, Euro-Mediterranean J. Environ. Integr. (2024) 1–14.
[31] S. Holdenrieder, P. Stieber, Apoptotic markers in cancer, Clin. Biochem. 37 (2004) 605–617, https://doi.org/10.1016/j.clinbiochem.2004.05.003.
[32] O. Boualam, S. El Alami, H. Ibaghlin, C. Chadli, K. Tanji, A. El Gaidoumi, R. Belaabed, H. Elknidri, A. Kherbeche, A. Addaou, Resourceful exploitation of sedimentary clay: designing a dual-chambered borosilicate glass reactor system for the efficient treatment of malachite green and phenol through SCRT adsorption and 5% Fe@ SRCT catalysis via CWPO, with evaluation of seed germination and fish survival, Water Environ. Res. 96 (2024) e11090.
[33] Y. Fahoul, K. Tanji, O.M.G. Díaz, R. Quesada-Cabrera, Y. Naciri, I. El Mrabet, A. El Gaidoumi, J.M.D. Rodríguez, A. Kherbeche, Development of a new CoS-Supported ZnAl2O4 catalyst for the visible photodegradation of a basic textile dye from water, Opt. Mater. 143 (2023) 114148.
[34] A. El Gaidoumi, A. Loqman, M. Zouheir, K. Tanji, O. Mertah, A. Dra, B. El Bali, A. Kherbeche, Sol–gel fluorinated TiO 2–clay nanocomposite: study of fluor-titanium interaction on the photodegradation of phenol, Res. Chem. Intermed. 47 (2021) 5203–5228.
[35] M. Sala, M.C. Gutiérrez-Bouzán, Electrochemical techniques in textile processes and wastewater treatment, Int. J. Photoenergy 2012 (2012).
[36] E.K. Paleologos, D.L. Giokas, M.I. Karayannis, Micelle-mediated separation and cloud-point extraction, TrAC Trends Anal. Chem. 24 (2005) 426–436.
[37] W.I. Mortada, M.M. Hassanien, A.A. El-Asmy, Cloud point extraction of some precious metals using Triton X-114 and a thioamide derivative with a salting-out effect, Egypt, J. Basic Appl. Sci. 1 (2014) 184–191.
[38] H. Tavallali, S. Yazdandoust, M. Yazdandoust, Cloud point extraction for the preconcentration of silver and palladium in real samples and determination by atomic absorption spectrometry, CLEAN–Soil, Air, Water 38 (2010) 242–247.
[39] y D. Mers, Surfactant Science and Technology, John Wiley & Sons, 2020.
[40] H. Isawi, Using zeolite/polyvinyl alcohol/sodium alginate nanocomposite beads for removal of some heavy metals from wastewater, Arab. J. Chem. 13 (2020) 5691–5716.
[41] S. Zaidi, T. Chaabane, V. Sivasankar, A. Darchen, R. Maachi, T.A.M. Msagati, Electro-coagulation coupled electro-flotation process: feasible choice in doxycycline removal from pharmaceutical effluents, Arab. J. Chem. 12 (2019) 2798–2809.

[42] B. Haddou, J.-P. Canselier, C. Gourdon, Use of cloud point extraction with ethoxylated surfactants for organic pollution removal, in: Role Colloid. Syst. Environ. Prot., Elsevier, 2014, pp. 97–142.
[43] M.K. Purkait, S.S. Vijay, S. DasGupta, S. De, Separation of Congo red by surfactant mediated cloud point extraction, Dye. Pigment. 63 (2004) 151–159.
[44] M.K. Purkait, S. Banerjee, S. Mewara, S. DasGupta, S. De, Cloud point extraction of toxic eosin dye using Triton X-100 as nonionic surfactant, Water Res. 39 (2005) 3885–3890.
[45] P. Taechangam, J.F. Scamehorn, S. Osuwan, T. Rirksomboon, Effect of nonionic surfactant molecular structure on cloud point extraction of phenol from wastewater, Colloids Surfaces A Physicochem. Eng. Asp. 347 (2009) 200–209.
[46] R.P.F. Melo, E.L.B. Neto, M. Moura, T.N.C. Dantas, A.A.D. Neto, H.N.M. de Oliveira, Removal of Reactive Blue 19 using nonionic surfactant in cloud point extraction, Sep. Purif. Technol. 138 (2014) 71–76.
[47] A. Appusamy, I. John, K. Ponnusamy, A. Ramalingam, Removal of crystal violet dye from aqueous solution using triton X-114 surfactant via cloud point extraction, Eng. Sci. Technol. an Int. J. 17 (2014) 137–144.
[48] T.G. Kazi, M. Tuzen, Magnetic stirrer induced dispersive ionic-liquid microextraction for the determination of vanadium in water and food samples prior to graphite furnace atomic absorption spectrometry, Food Chem. 172 (2015) 161–165.
[49] H. Reffas, T. Benabdallah, M.H. Youcef, H. Ilikti, Removal of copper (II) from a concentrated sulphate medium by cloud point extraction using an N, N′-Bis (salicylaldehyde) ethylenediimine di-schiff base chelating ligand, J. Surfactants Deterg. 17 (2014) 27–35.
[50] W. Liu, W. Zhao, J. Chen, M. Yang, A cloud point extraction approach using Triton X-100 for the separation and preconcentration of Sudan dyes in chilli powder, Anal. Chim. Acta 605 (2007) 41–45.
[51] Z. Pourghobadi, R. Heydari, R. Pourghobadi, M. Rashidipour, Determination of gabapentin in human plasma using simultaneous cloud point extraction and precolumn derivatization by HPLC, Monatshefte Für Chemie-Chemical Mon 144 (2013) 773–779.
[52] S.S. Arya, A.M. Kaimal, M. Chib, S.K. Sonawane, P.L. Show, Novel, energy efficient and green cloud point extraction: technology and applications in food processing, J. Food Sci. Technol. 56 (2019) 524–534.
[53] B.A. de Marco, B.S. Rechelo, E.G. Tótoli, A.C. Kogawa, H.R.N. Salgado, Evolution of green chemistry and its multidimensional impacts: a review, Saudi Pharm. J. 27 (2019) 1–8.
[54] M.R. Al_Saadi, Z.S. Al-Garawi, M.Z. Thani, Promising technique, cloud point extraction: technology & applications, in: J. Phys. Conf. Ser., IOP Publishing, 2021 12064.
[55] D. Snigur, E.A. Azooz, O. Zhukovetska, O. Guzenko, W. Mortada, Recent innovations in cloud point extraction towards a more efficient and environmentally friendly procedure, TrAC Trends Anal. Chem. 164 (2023) 117113.
[56] R.K. Ridha, D.H. Alasady, E.A. Azooz, W.I. Mortada, Rapid synergistic cloud point extraction based on hydrophobic deep eutectic solvent combined with hydride generation atomic absorption spectrometry for determination of selenium in tea samples, J. Food Compos. Anal. 132 (2024) 106286.
[57] G.J. Shabaa, F.A. Semysim, R.K. Ridha, E.A. Azooz, E.A.J. Al-Mulla, Air-assisted dual-cloud point extraction coupled with flame atomic absorption spectroscopy for the separation and quantification of zinc in pregnant women's serum, J. Iran. Chem. Soc. 20 (2023) 2277–2284.
[58] J. Zolgharnein, M. Bagtash, T. Shariatmanesh, Simultaneous removal of binary mixture of Brilliant Green and Crystal Violet using derivative spectrophotometric determination, multivariate optimization and adsorption characterization of dyes on surfactant modified nano-γ-alumina, Spectrochim. Acta Part A Mol. Biomol. Spectrosc. 137 (2015) 1016–1028.
[59] M. Turabik, Adsorption of basic dyes from single and binary component systems onto bentonite: simultaneous analysis of Basic Red 46 and Basic Yellow 28 by first order derivative spectrophotometric analysis method, J. Hazard Mater. 158 (2008) 52–64.
[60] S. Sallam, M. Aljohani, N.M. Alatawi, H. Alsharief, S.F. Ibarhiam, A. Almahri, R.B. Alnoman, N.M. El-Metwaly, Box-Behnken design optimization of bimetallic-organic frameworks for effective removal of tartrazine food dye from aqueous solutions, J. Mol. Liq. 393 (2024) 123667.
[61] W.I. Mortada, Recent developments and applications of cloud point extraction: a critical review, Microchem. J. 157 (2020) 105055.
[62] M. Alipour, M. Vosoughi, S.A. Mokhtari, H. Sadeghi, Y. Rashtbari, M. Shirmardi, R. Azad, Optimising the basic violet 16 adsorption from aqueous solutions by magnetic graphene oxide using the response surface model based on the Box–Behnken design, Int. J. Environ. Anal. Chem. 101 (2021) 758–777.
[63] B. Gözmen, M. Turabik, A. Hesenov, Photocatalytic degradation of Basic Red 46 and Basic Yellow 28 in single and binary mixture by UV/TiO2/periodate system, J. Hazard Mater. 164 (2009) 1487–1495.
[64] E. Sharifpour, P. Arabkhani, F. Sadegh, A. Mousavizadeh, A. Asfaram, In-situ hydrothermal synthesis of CNT decorated by nano ZnS/CuO for simultaneous removal of acid food dyes from binary water samples, Sci. Rep. 12 (2022) 12381.
[65] A. Asfaram, M. Ghaedi, G.R. Ghezelbash, F. Pepe, Application of experimental design and derivative spectrophotometry methods in optimization and analysis of biosorption of binary mixtures of basic dyes from aqueous solutions, Ecotoxicol. Environ. Saf. 139 (2017) 219–227.
[66] A. Asfaram, M. Ghaedi, F. Yousefi, M. Dastkhoon, Experimental design and modeling of ultrasound assisted simultaneous adsorption of cationic dyes onto ZnS: Mn-NPs-AC from binary mixture, Ultrason. Sonochem. 33 (2016) 77–89.
[67] S. Choudhury, S.K. Ray, Efficient removal of cationic dye mixtures from water using a bio-composite adsorbent optimized with response surface methodology, Carbohydr. Polym. 200 (2018) 305–320.
[68] T. Güray, B. Menevşe, A.A. Yavuz, Determination of optimization parameters based on the Box-Behnken design for cloud point extraction of quinoline yellow using Brij 58 and application of this method to real samples, Spectrochim. Acta Part A Mol. Biomol. Spectrosc. 243 (2020) 118800.
[69] S.L.C. Ferreira, M.M.S. Junior, C.S.A. Felix, D.L.F. da Silva, A.S. Santos, J.H.S. Neto, C.T. de Souza, R.A.C. Junior, A.S. Souza, Multivariate optimization techniques in food analysis–A review, Food Chem. 273 (2019) 3–8.
[70] A. El Gaidoumi, K. Tanji, A. Loqman, I. El Mrabet, A. Arrahli, A. Dra, Y. Fahoul, M. Zouheir, B. El Bali, A. Kherbeche, Cu (II) impregnated clay-derived HS zeolite: synthesis, characterization and catalytic activity on catalytic wet peroxide oxidation (CWPO) of phenol, J. Coord. Chem. 75 (2022) 2710–2731.
[71] A. El Gaidoumi, A. Loqman, A.C. Benadallah, B. El Bali, A. Kherbeche, Co (II)-pyrophyllite as catalyst for phenol oxidative degradation: optimization study using response surface methodology, Waste and Biomass Valorization 10 (2019) 1043–1051.
[72] J. Zolgharnein, M. Rastgordani, Optimization of simultaneous removal of bi-nary mixture of and methyl orange dyes by cobalt hydroxide nanoparticles through Taguchi method, J. Mol. Liq. (2018).
[73] J. Zolgharnein, M. Rastgordani, Multivariate optimization and characterization of simultaneous removal of binary mixture of Cu (II) and Pb (II) using Fe3O4@ MoS2 nanoparticles, J. Chemom. 32 (2018) e3043.
[74] M. Mäkelä, Experimental design and response surface methodology in energy applications: a tutorial review, Energy Convers. Manag. 151 (2017) 630–640.
[75] E. Natarajan, G.P. Ponnaiah, Optimization of process parameters for the decolorization of Reactive Blue 235 dye by barium alginate immobilized iron nanoparticles synthesized from aluminum industry waste, Environ. Nanotechnology, Monit. Manag. 7 (2017) 73–88.
[76] A. Dra, K. Khallouk, K. Tanji, I. El Mrabet, Y. Fahoul, B. El Fathi, A. Arrahli, A. El Gaidoumi, L. Mardi, A. Taleb, Removal of crystal violet dye from aqueous solution using oued sebou sediment (Fez-Morocco): Box-Behnken optimization and germination studies, Water, Air, Soil Pollut. 234 (2023) 87.
[77] H. Souhassou, K. Khallouk, R. El Khalfaouy, A. El Gaidoumi, L. Nahali, Y. Fahoul, K. Tanji, A. Kherbeche, Optimization of a binary dye mixture adsorption by Moroccan clay using the box-behnken experimental design, Chem. Africa 6 (2023) 2011–2027.
[78] J. Smith, Chemical Engineering Kinetics, 3nd edn, McGraw-Hill, New York, 1981.
[79] M. Ghaedi, M. Montazerozohori, M.N. Biyareh, K. Mortazavi, M. Soylak, Chemically bonded multiwalled carbon nanotubes as efficient material for solid phase extraction of some metal ions in food samples, Int. J. Environ. Anal. Chem. 93 (2013) 528–542.
[80] N.M. Mahmoodi, R. Salehi, M. Arami, H. Bahrami, Dye removal from colored textile wastewater using chitosan in binary systems, Desalination 267 (2011) 64–72.
[81] A. Kurniawan, H. Sutiono, N. Indraswati, S. Ismadji, Removal of basic dyes in binary system by adsorption using rarasaponin–bentonite: revisited of extended Langmuir model, Chem. Eng. J. 189 (2012) 264–274.
[82] M. Arabi, M. Ghaedi, A. Ostovan, Development of a lower toxic approach based on green synthesis of water-compatible molecularly imprinted nanoparticles for the extraction of hydrochlorothiazide from human urine, ACS Sustain. Chem. Eng. 5 (2017) 3775–3785.

[83] S. Lagergren, Zur theorie der sogenannten adsorption gelöster stoffe, K Sven Vetenskapsakad. Handl 24: 1–39 38 Ho YS, McKay G (1999) Pseudo-second order model for sorption processes, Proc Biochem 34 (1898) 451–465.
[84] Y.-S. Ho, G. McKay, Sorption of dye from aqueous solution by peat, Chem. Eng. J. 70 (1998) 115–124.
[85] R.P.F. Melo, E.L. de Barros Neto, M.C.P. de A. Moura, T.N. de Castro Dantas, A.A. Dantas Neto, S.K. da S. Nunes, Removal of Direct Yellow 27 dye by ionic flocculation: the use of an environmentally friendly surfactant, J. Surfactants Deterg. 20 (2017) 459–465.
[86] C. Puri, G. Sumana, Highly effective adsorption of crystal violet dye from contaminated water using graphene oxide intercalated montmorillonite nanocomposite, Appl. Clay Sci. 166 (2018) 102–112.
[87] J.L. Marco-Brown, L. Guz, M.S. Olivelli, B. Schampera, R.M.T. Sánchez, G. Curutchet, R. Candal, New insights on crystal violet dye adsorption on montmorillonite: kinetics and surface complexes studies, Chem. Eng. J. 333 (2018) 495–504.
[88] M.M. Hamed, R.F. Aglan, Removal of Arsenazo-III from liquid radioactive waste by cloud point extraction, J. Radioanal. Nucl. Chem. 321 (2019) 917–926.
[89] A.M. Omer, G.S. Elgarhy, G.M. El-Subruiti, R.E. Khalifa, A.S. Eltaweil, Fabrication of novel iminodiacetic acid-functionalized carboxymethyl cellulose microbeads for efficient removal of cationic crystal violet dye from aqueous solutions, Int. J. Biol. Macromol. 148 (2020) 1072–1083.
[90] Z. Rawajfih, N. Nsour, Adsorption of γ-picoline onto acid-activated bentonite from aqueous solution, Appl. Clay Sci. 47 (2010) 421–427.
[91] M.M. Hamed, M. Holiel, Z.H. Ismail, Removal of 134Cs and 152+ 154Eu from liquid radioactive waste using Dowex HCR-S/S, Radiochim, Acta 104 (2016) 399–413.
[92] M.M. Hamed, H.E. Rizk, I.M. Ahmed, Adsorption behavior of zirconium and molybdenum from nitric acid medium using low-cost adsorbent, J. Mol. Liq. 249 (2018) 361–370.
[93] H. Shayesteh, A. Rahbar-Kelishami, R. Norouzbeigi, Evaluation of natural and cationic surfactant modified pumice for Congo red removal in batch mode: kinetic, equilibrium, and thermodynamic studies, J. Mol. Liq. 221 (2016) 1–11.
[94] R. Bhuvaneswari, K. Arivalagan, R. Tamilarasan, Isotherms, kinetics and thermodynamics of adsorption study in dye removal of Albizzia Leb-beck seed activated carbon, Int J Innov Res Adv Stud 4 (2017) 108–113.
[95] Z. Zhang, J. Kong, Novel magnetic Fe3O4@ C nanoparticles as adsorbents for removal of organic dyes from aqueous solution, J. Hazard Mater. 193 (2011) 325–329.
[96] S. Marghzari, M. Sasani, M. Kaykhaii, M. Sargazi, M. Hashemi, Simultaneous elimination of malachite green, rhodamine B and cresol red from aqueous sample with sistan sand, optimized by taguchi L16 and plackett–burman experiment design methods, Chem. Cent. J. 12 (2018) 1–11.
[97] Z. Ahamad, A. Nasar, Polypyrrole-decorated bentonite magnetic nanocomposite: a green approach for adsorption of anionic methyl orange and cationic crystal violet dyes from contaminated water, Environ. Res. 247 (2024) 118193.
[98] J. Hu, B. Mi, L. Chen, Y. Yuan, J. Zhang, F. Wu, An economical preparation strategy of magnetic biochar with high specific surface area for efficient removal of methyl orange, Int. J. Biol. Macromol. 276 (2024) 134156.
[99] S. Pradhan, N.S. Anuraag, N. Jatav, I. Sinha, N.K. Prasad, Magnetic Ni@ C nanoadsorbents for methyl orange removal from water, Environ. Sci. Pollut. Res. 30 (2023) 118634–118646.
[100] Q. Liu, G.-L. Zang, Q. Zhao, Removal of methyl orange wastewater by Ugi multicomponent reaction functionalized UiO-66-NS, Environ. Sci. Pollut. Res. 29 (2022) 76833–76846.
[101] T.-S. Guo, S.-D. Yang, H.-M. Cui, Q.-F. Yu, M.-F. Li, Synthesis of lignin nanoparticle-manganese dioxide complex and its adsorption of methyl orange, Int. J. Biol. Macromol. 253 (2023) 127012.
[102] U. Ghani, K. Hina, M. Iqbal, M.K. Irshad, I. Aslam, R. Saeed, M. Ibrahim, Kinetic and isotherms modeling of methyl orange and chromium (VI) onto hexagonal ZnO microstructures as a membrane for environmental remediation of wastewater, Chemosphere 309 (2022) 136681.
[103] N. Tahari, P.L. de Hoyos-Martinez, N. Izaguirre, N. Houwaida, M. Abderrabba, S. Ayadi, J. Labidi, Preparation of chitosan/tannin and montmorillonite films as adsorbents for Methyl Orange dye removal, Int. J. Biol. Macromol. 210 (2022) 94–106.
[104] B. Zhu, J. Xu, Z. Xu, M. Wu, H. Jiang, Soft-template solvent thermal method synthesis of magnetic mesoporous carbon–silica composite for adsorption of methyl orange from aqueous solution, Environ. Sci. Pollut. Res. 29 (2022) 40734–40744.
[105] M.U. Herrera, C.M. Futalan, R. Gapusan, M.D.L. Balela, Removal of methyl orange dye and copper (II) ions from aqueous solution using polyaniline-coated kapok (Ceiba pentandra) fibers, Water Sci. Technol. 78 (2018) 1137–1147.
[106] S.E. Rizk, M.M. Hamed, Batch sorption of iron complex dye, naphthol green B, from wastewater on charcoal, kaolinite, and tafla, Desalin. Water Treat. 56 (2015) 1536–1546.